Geodesic Distance Based Scattering Power Decomposition for Compact Polarimetric SAR Data

Arnab Muhuri, Kalifa Goïta, Ramata Magagi, and Hongquan Wang

***Abstract*— We propose a geodesic distance (GD)-based scattering power decomposition for compact polarimetric (CP) synthetic aperture radar (SAR) data acquired over agricultural landscapes. The proposed technique decomposes the polarized portion of the total backscattered power in proportion to the normalized target similarity measures. The measures are derived from the GDs, which are computed between the Kennaugh matrices of observed and canonical targets (dihedral or trihedral). We observed a pseudo-power component in the double bounce power, which can be attributed to target irregularities. To compensate for the pseudo-power component, we proposed a compensation strategy by utilizing the CP radar vegetation index (CpRVI). The compensation factor assists in readjusting the polarized power components. The proposed approach was tested with real (RADARSAT Constellation Mission: RCM) and simulated (RADARSAT-2: RS2) hybrid CP data over agricultural sites in Canada. The effectiveness of the approach was demonstrated by comparing the decomposed powers with a recently proposed CP scattering power decomposition.**

***Index Terms*— Canonical targets, compact polarimetric (CP) synthetic aperture radar (SAR) decomposition, geodesic distance (GD), RADARSAT-2 (RS2), RADARSAT Constellation Mission (RCM).**

I. Introduction

TARGET decomposition techniques are crucial for understanding the scattering mechanisms in polarimetric synthetic aperture radar (PolSAR) observations. Such techniques are useful for associating a physical scattering mechanism to each component of the decomposed backscattered radar power [1], [2], [3], [4], [5], [6]. Various strategies ranging from model-based decomposition (MBD) to eigenvector-based decomposition (EVBD) have been employed for decomposing the PolSAR data [7], [8], [9], [10].

In the domain of image and signal processing, the idea of utilizing a distance and divergence measure to assess the proximity of pixel samples to a reference characteristic is reasonably well known [11], [12]. Classification of PolSAR data based on the symmetric scatterer space distance measure from canonical targets was proposed in Cameron's classification scheme [13], [14]. Speckle reduction and edge detection in PolSAR images were achieved using approaches based on the concept of stochastic distance between complex Wishart distributions [15], [16]. An investigation employed the Hellinger distance to estimate the polarization orientation angle for compensating for the pseudo-decomposition power (in the volume scattering) arising from rotated urban areas [17]. The concept of geodesic distance (GD) [18] has been utilized in a different manner for feature extraction, region discrimination, and texture retrieval in PolSAR images [19], [20]. Recent investigations exploited the concept of temporal changes in the PolSAR scattering mechanisms [21], [22], [23] and utilized the idea of GD for computing the distance between the Kennaugh matrices of the observed and canonical/elementary targets for mapping urban change detection [24]. A generalized radar vegetation index (GRVI) was proposed based on the concept of GD [24] between the Kennaugh matrix corresponding to the generalized volume scattering model (GVSM) (K_v) [25] and the observed Kennaugh matrix (K_{Target}) associated with the PolSAR backscattering from the vegetation [26], [27].

Even though full/quad polarimetric (FP) SAR data has been repeatedly acknowledged for providing superior-quality radar observations, such systems are operated at a reduced swath width due to the large volume of the acquired data. On the other hand, compact polarimetric (CP) systems provide a middle ground by covering twice the swath width of FP systems and greater polarization information when compared to dual-polarimetric (DP) linear systems [28]. One of the manifestations of CP, the hybrid CP mode, transmits right- or left-handed circular polarization and receives in linear polarization (circular transmit linear receive: CTLR). The hybrid CP mode demonstrates some engineering advantages such as the ease of implementation, self-calibration capability, and lower susceptibility to noise and cross-channel errors,

Manuscript received 13 January 2023; revised 21 March 2023 and 3 August 2023; accepted 8 August 2023. Date of publication 14 August 2023; date of current version 15 September 2023. This work was supported in part by the Natural Science and Engineering Research Council of Canada (NSERC) Discovery under Grant RGPIN-2017-05533 and Grant RGPIN-2018-06101, in part by Collaborative Research and Training Experience (CREATE) under Grant 543360-2020, and in part by the Canadian Space Agency Class Grant and Contribution Program under Grant 21SUESAMMI as part of the Canadian plan to spatial missions of soil moisture. *(Corresponding author: Arnab Muhuri.)*

Arnab Muhuri was with the Centre d'Applications et de Recherches en Télédétection (CARTEL), Département de Géomatique Appliquée, Université de Sherbrooke, Sherbrooke, QC J1K 2R1, Canada. He is now with the Earth Observation and Modelling (EOM), Geographisches Institut, Christian-Albrechts-Universität zu Kiel, Kiel, 24118 Schleswig-Holstein, Germany (e-mail: muhuri@geographie.uni-kiel.de).

Kalifa Goïta and Ramata Magagi are with the Centre d'Applications et de Recherches en Télédétection (CARTEL), Département de Géomatique Appliquée, Université de Sherbrooke, Sherbrooke, QC J1K 2R1, Canada.

Hongquan Wang was with the Centre d'Applications et de Recherches en Télédétection (CARTEL), Département de Géomatique Appliquée, Université de Sherbrooke, Sherbrooke, QC J1K 2R1, Canada. He is now with the Lethbridge Research and Development Centre, Agriculture and Agri-Food Canada (AAFC), 5403 1 Ave S, Lethbridge, AB T1J 4B1, Canada.

Digital Object Identifier 10.1109/TGRS.2023.3304710

which leads to the superior quality of CP data [29]. The CTLR mode defies the conventional idea of having a dual-circularly polarized on receive (same sense and opposite sense) for a circularly polarized transmit. This convention is based on the traditionally followed design agreement for the transmit and the receive basis (linear or circular). However, the fundamental principles assure conservation of the backscattered power from a target only when the power is split into an orthogonal pair of polarization. This is possible only if the received polarization has no like or cross-polarized relationship to the transmitted polarization. Consequently, this serves as the fundamental idea of having the received polarization on a linear basis even though the transmitted polarization is on a circular basis for a CTLR system. This seemingly contrarian transmit–receive architecture has been observed to be impartially superior to other proposed alternatives for a CP system [30], [31].

Although several strategies have been explored with CP SAR data for decomposing the total backscattered power, the distance based approach still largely remains unexplored [32], [33], [34], [35], [36], [37]. In this investigation, we exploited the concept of GD between the Kennaugh matrices of the canonical and the observed targets to decompose the total polarized power. Furthermore, for readjusting the powers in the polarized components, we proposed a strategy to compute a pseudo-power compensation factor by utilizing the CP radar vegetation index (CpRVI) [38]. This was crucial since we noticed unreasonable levels of double bounce power over the agricultural fields even under bare field conditions. The effectiveness of the proposed decomposition was demonstrated with real hybrid compact RADARSAT Constellation Mission (RCM) and simulated RADARSAT-2 (RS2) data for various crop types. The proposed decomposition powers closely matched the CP decomposition proposed by [35].

II. Test Site and Data

A. Test Site and In Situ Measurements

1) Sherbrooke (RCM Data, 2022), Québec, Canada: The Sherbrooke Research and Development Centre is located in Sherbrooke, QC, Canada, and serves as one of the Agriculture and Agri-Food Canada's (AAFC) network of 20 research and development centers. The center is surrounded by experimental agricultural fields growing a variety of crops like soya, corn, and wheat. We conducted a detailed field campaign in 2022 and continuously monitored the fields using a soil moisture sensor network and periodic field measurements of vital parameters such as crop biomass, vegetation growth stage, and soil moisture, which were synchronized with RCM, RS2, and Sentinel-1 (S1) satellite passes.

2) Carman (RS2 Data, 2016), Manitoba, Canada: Carman is an important agricultural hub in Manitoba, Canada, due to the presence of a wide variety of agricultural businesses and services within easy access to national and international logistics and transportation corridors. The region is located in the middle of a rich agricultural belt approximately 90 km west of Winnipeg and 60 km north of the US border at the eastern edge of the Canadian prairies. This site was part of the SMAPVEX 2012 and 2016 field campaigns, when the fields were monitored regularly with a variety of field sensor networks from AAFC, US Department of Agriculture (USDA), and a variety of manual measurements. We selected fields planted with soya and corn for our investigation since they were common crop types between both sites. These fields were sown in early May and harvested toward late September or early October.

TABLE I
SATELLITE SAR TIME-SERIES OVER THE TEST SITES. RS2 (FOR SIMULATED HYBRID CP DATA; FQ15W: 33.78°–36.37°) AND RCM (FOR REAL HYBRID CP DATA; SCANSAR: 17.03°–21.90°). *D*1, *D*2, AND *D*3 INDICATE TEMPORAL PROGRESSION OF CROP GROWTH

SAR Satellite Sensor	D1	D2	D3
RCM (Sherbrooke, Québec, 2022)	24th June	14th July	7th August
RS2 (Carman, Manitoba, 2016)	16th May	9th June	27th July

B. Satellite Data

1) RCM (For Real Hybrid CP Data): RCM is Canada's state-of-the-art Earth observation constellation mission consisting of three identical satellites operating at C-band, which provides near real-time observations over Canada. The hybrid CP CTLR mode of RCM transmits a right-handed circular (RHC) polarization and receives in linear polarizations (horizontal: H and vertical: V). The circular transmit polarization is achieved by simultaneously transmitting H and V polarizations, which are 90° out of phase [29]. This imaging mode enables a wider swath/coverage when compared to FP SAR systems. The data supplied in the form of 2×2 complex covariance (C) matrices are utilized to compute the Stokes vectors and Kennaugh matrices. We utilized the RCM data available over the Sherbrooke test site covering a cropping cycle in 2022, as listed in Table I. The crop growth over the soya and corn fields can be observed in Fig. 1.

2) RS2 (For Simulated Hybrid CP Data): RS2 is one of the world's most advanced Canadian satellite SAR systems with FP capabilities operating at C-band. FP SAR systems separately transmit orthogonally polarized radar pulses (horizontal: H and vertical: V) and measure the backscattered signal in both polarizations [39]. Each pixel of FP data is characterized by a complex scattering matrix, which relates the incident and the backscattered wave [40]. In the absence of real hybrid CP data, the FP data can be utilized to simulate a CTLR Stokes vector as per the first principles presented in [29]. We employed the RS2 data available over the Carman test site covering a cropping cycle in 2016, as listed in Table I. The crop growth over the soya and corn fields can be observed in Fig. 2.

C. Crop Characteristics

Crop characteristics influence the performance of satellite data-derived vegetation descriptors such as CpRVI, which are utilized for capturing the crop growth dynamics at different phenological stages. Therefore, clarity on the structural attributes of the crops is essential. The agricultural fields considered for this investigation were planted with the following crop types.

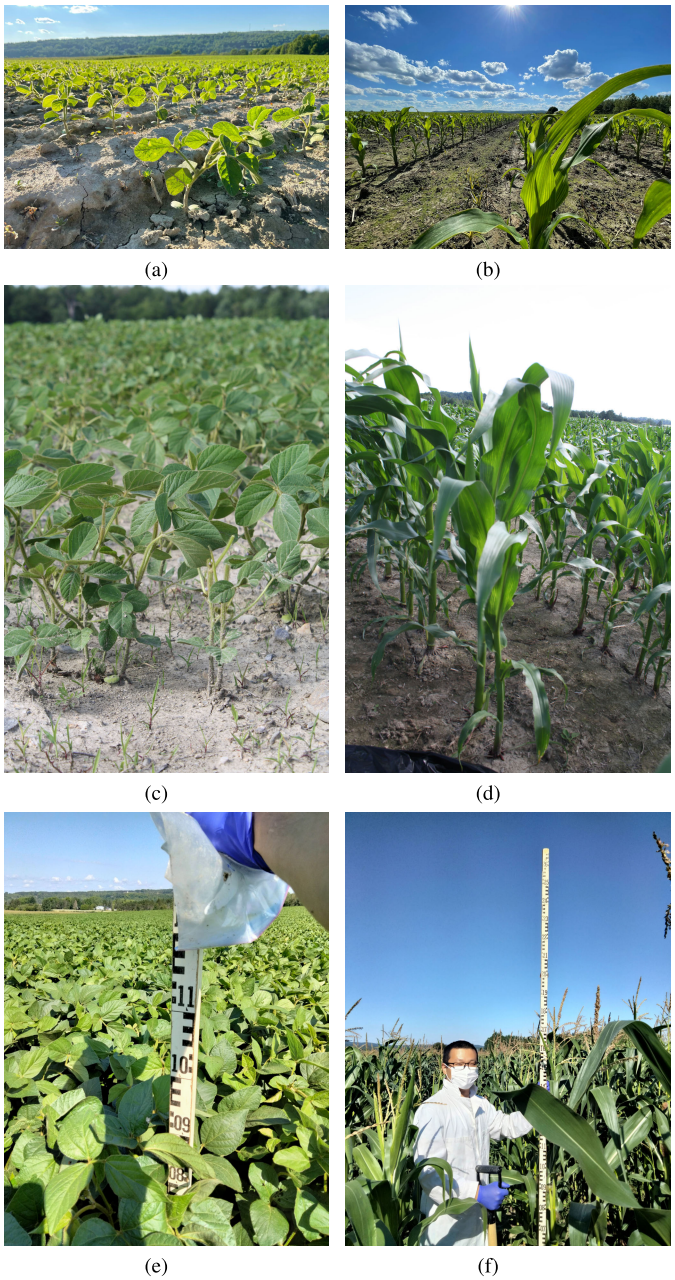

Fig. 1. Temporal progression of crop growth over a soya and corn field: Sherbrooke, QC, Canada, 2022. (e) and (f) Vegetation height over the soya and corn fields in the advanced stage of crop growth, respectively. Site for RCM real hybrid CP data. (a) Soya: 24th June. (b) Corn: 24th June. (c) Soya: 16th July. (d) Corn: 16th July. (e) Soya: 1st August. (f) Corn: 1st August.

Fig. 2. Temporal progression of crop growth over a soya and corn field: Carman, MB, Canada, 2016. Fields were sown early in May, which explains the vegetation-free bare conditions. Site for RS2-simulated hybrid CP data. (a) Soya: 16th May. (b) Corn: 16th May. (c) Soya: 9th June. (d) Corn: 9th June. (e) Soya: 27th July. (f) Corn: 27th July.

1) Soya: The soya plant develops as a pair of single blades, which subsequently branches out to matured nodes with compounded leaves with three blades. These further mature into trifoliolate leaves consisting of 3–4 leaflets per leaf, which are 6–15 cm long and 2–7 cm broad. The leafing stages are followed by flowering, full bloom, beginning and full pod, beginning and full seed, and physiological maturity [41]. In its matured stage, the plant reaches 50–125 cm in height [Fig. 1(e)].

2) Corn: A well-developed corn plant is often 3 m or taller in height [Fig. 1(f)] and the spiked ears (female flowers), with the corn kernels encased in sheaths of leaves, develop in the midsection of the plant. It is composed of leaves sprouting from the nodes, alternately on opposite sides of the stalk with the stem divided into several internodes. The growth stages of corn can be majorly classified into vegetative or reproductive. After emergence, the development of the leaves with fully developed collars is followed by the development of tassels (male flowers), which ends the vegetative leafing stage [42]. The planting density of corn affects multiple factors such as the number of ears per stalk and plant matter (important for silage).

III. Methodology

The hybrid CP SAR observation is expressed as 4×1 Stokes vector [see (1)], which is derived from the 2×2 complex covariance (C) matrix as

$$S = \begin{bmatrix} S_0 \\ S_1 \\ S_2 \\ S_3 \end{bmatrix} = \begin{bmatrix} C_{11} + C_{22} \\ C_{11} - C_{22} \\ C_{12} + C_{21} \\ \pm j(C_{12} - C_{21}) \end{bmatrix} \tag{1}$$

where $\pm$ corresponds to the left-hand circular (LHC: $+$) or right-hand circular (RHC: $-$) transmitted signal in the hybrid CP mode. The transmitted and the received Stokes vectors are related to the Kennaugh matrix, which was introduced by [43] for evaluating the power received in a radar observation.

The hybrid CP SAR Kennaugh matrix can be expressed in terms of the elements of the Stokes vector as

$$K = \begin{bmatrix} S_0 & 0 & S_2/2 & 0 \\ 0 & 0 & 0 & S_1 \\ S_2/2 & 0 & 0 & 0 \\ 0 & S_1 & 0 & S_3/2 \end{bmatrix}. \tag{2}$$

To decompose the polarized component of the backscattered power, we utilized the concept of GD, which is computed as

$$\mathrm{GD}(K_1, K_2) = \frac{2}{\pi} \cos^{-1} \frac{\mathrm{Tr}\left(K_1^T K_2\right)}{\sqrt{\mathrm{Tr}\left(K_1^T K_1\right)}\sqrt{\mathrm{Tr}\left(K_2^T K_2\right)}} \tag{3}$$

where K_1 and K_2 are the two Kennaugh matrices for the canonical (K_{Dihedral} or $K_{\mathrm{Trihedral}}$) and real targets (K_{Target}), respectively. Tr and T are the trace and transpose operators, respectively. Factor $(2/\pi)$ normalizes the distance GD in the range 0–1. We consider the canonical Kennaugh matrices for the dihedral and trihedral targets due to their close association with even and odd bounce scatterings, respectively. A similarity measure between the real and the canonical targets is the inverse of GD, which was computed as

$$\mathrm{SIM}_{\mathrm{DB}} = 1 - \mathrm{GD}\left(K_{\mathrm{Dihedral}}, K_{\mathrm{Target}}\right) \tag{4.1}$$

$$\mathrm{SIM}_S = 1 - \mathrm{GD}\left(K_{\mathrm{Trihedral}}, K_{\mathrm{Target}}\right). \tag{4.2}$$

In the proposed decomposition, the randomly polarized volume power (P_V) is computed as the fraction of the total backscattered power that is depolarized ($1 - \mathrm{DoP}$) during the process of radar signal scattering. This is a popular formulation followed by past investigations [33], [34], [35]. The degree of polarization (DoP) [44] is computed as

$$\mathrm{DoP} = \frac{\sqrt{S_1^2 + S_2^2 + S_3^2}}{S_0}. \tag{5}$$

We introduced the idea of distance based decomposition for dividing the polarized power component into two elementary scattering mechanisms (surface: P_S and double bounce: P_{DB}). The polarized powers (P_{DB} and P_S) were computed by bifurcating the total polarized power ($S_0 \times \mathrm{DoP}$) in proportion to the normalized similarity measures with respect to the canonical targets (dihedral or trihedral). The normalized similarity measures [dihedral similarity: $(\mathrm{SIM}_{\mathrm{DB}})/(\mathrm{SIM}_{\mathrm{DB}}+\mathrm{SIM}_S)$ and trihedral similarity: $(\mathrm{SIM}_S)/(\mathrm{SIM}_{\mathrm{DB}} + \mathrm{SIM}_S)$] vary from 0 to 1, spanning the lowest to highest level of similarity of the observed target to the canonical targets, respectively. The proposed decomposition powers were computed as

$$P_V = S_0 \times (1 - \mathrm{DoP}) \tag{6.1}$$

$$P_{\mathrm{DB}} = S_0 \times \mathrm{DoP} \times \frac{\mathrm{SIM}_{\mathrm{DB}}}{\mathrm{SIM}_{\mathrm{DB}} + \mathrm{SIM}_S} \tag{6.2}$$

$$P_S = S_0 \times \mathrm{DoP} \times \frac{\mathrm{SIM}_S}{\mathrm{SIM}_{\mathrm{DB}} + \mathrm{SIM}_S}. \tag{6.3}$$

With the distance based decomposition, we observed unreasonable levels of double bounce power over the agricultural fields. We hypothesized that there was a presence of a pseudo-power component due to target irregularities that was causing this overestimation. Target irregularities play a role in determining the randomness (between even or odd bounce and nonspecular scattering contributions) of the scattering process [45], [46]. While a perfectly smooth surface scatters the incident signal in the specular direction, a surface (and subsurface) with irregularities scatters the signal in all directions following the Lambertian law [47], [48]. Under such circumstances, we realized that a readjustment between the polarized powers (P_{DB} and P_S) was necessary. Therefore, we proposed to compute a compensation factor (P_{Extra}) from the double bounce component with an exponentially decaying function of CpRVI as

$$P_{\mathrm{Extra}} = P_{\mathrm{DB}} \times \exp(-\mathrm{CpRVI}). \tag{7}$$

It is important to note that this randomness in the scattering of the polarized powers is different from the randomness that occurs under vegetated conditions, where the latter causes depolarization (or nonconservation) of the total power that contributes to the diffused/volume scattering. Therefore, we utilized an exponentially decaying function of CpRVI to compute the pseudo-power component in the double bounce, which is caused as a result of randomness in the scattering of the polarized powers. The exponentially decreasing nature of compensation indicates that as the CpRVI increases, the idea of scattering randomness associated with the surface irregularities becomes less significant since the scattering tendency over the fields gradually shifts toward the volume/diffused power component arising from the signal interaction with the growing vegetation.

The CpRVI is derived using the concept of GD between the Kennaugh matrices of the observed target and an ideal depolarizer (ID), which is a realization of vegetation canopy [38], [49]. The distance is then utilized for computing a similarity measure, which is modulated with a scaled quantity that is derived from signal scattering power ratio of the same and opposite sense polarization [38]. The sense of polarization is determined with respect to the handedness (left or right) of the transmitted circular polarization. We utilized CpRVI as an indicator of the degree of readjustment/compensation that was necessary between the polarized components depending on the similarity of a target to an ID. Therefore, as the GD to the ID decreased (with the increase in the crop growth), the compensation requirement of the polarized components exponentially decreased as the power of CpRVI. The polarized components of the decomposed powers were readjusted using the P_{Extra} as

$$P_{\mathrm{DB}} = P_{\mathrm{DB}} - P_{\mathrm{Extra}} \tag{8.1}$$

$$P_S = P_S + P_{\mathrm{Extra}} \tag{8.2}$$

where P_{Extra} varies from 100% to 36.78% of P_{DB} as the CpRVI varies from 0 to 1, respectively.

We evaluated the proposed decomposition powers by comparing them with the recently proposed nonmodel-based three-component scattering power CP decomposition utilizing novel roll-invariant scattering-type parameters [35], which are known for their robustness under a change of wave polarization basis [4]. We observed the correlation between the crop growth information collected over the two agricultural sites and the change in the decomposition powers.

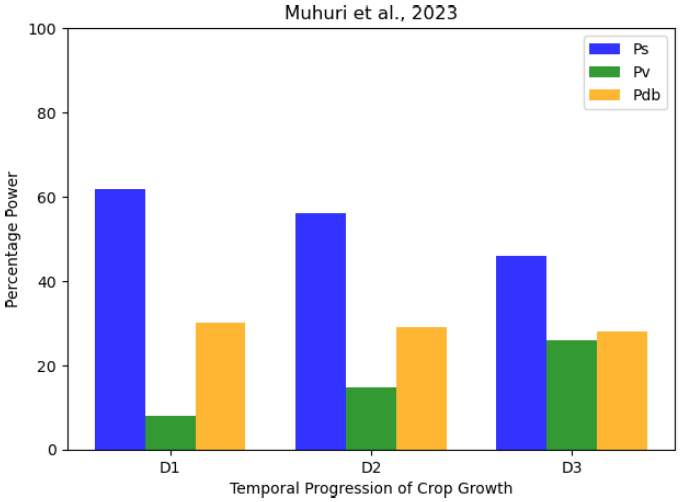

Fig. 3. Uncompensated decomposition powers over a soya field: Sherbrooke, QC, Canada, 2022. $D1$, $D2$, and $D3$ (as listed in Table I) indicate temporal progression of crop growth. The compensated powers are shown in Fig. 6(a). The powers are averaged over an agricultural field. Observations for RCM real hybrid CP data.

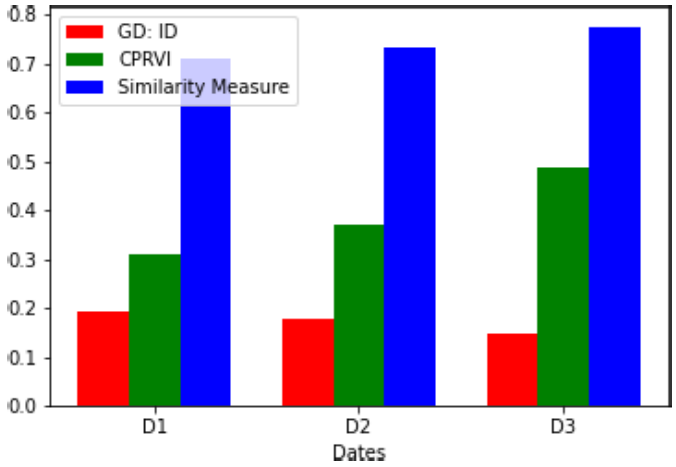

Fig. 4. Variation of CpRVI along with GD and SIM to an ID [38] over a soya field: Sherbrooke, QC, Canada, 2022. The corresponding uncompensated and compensated powers are shown in Figs. 3 and 6(a), respectively. $D1$: June, $D2$: July, and $D3$: August indicate temporal progression of the crop growth. The measures are averaged over an agricultural field. Observations for RCM real hybrid CP data.

IV. Results

We tested the proposed decomposition technique with real and simulated hybrid CP data over soya and corn fields, which were common crop types between the agricultural sites. With the preliminary distance based decomposition of the polarized powers [see (6.1)–(6.3)] in proportion to the similarity measures to the canonical targets (dihedral or trihedral), we noted an overestimation of the double bounce powers, as shown, for example, in Fig. 3 for a soya field. Upon comparison of our decomposed polarized powers with [35], we observed that our double bounce powers were overestimated, whereas the surface powers were underestimated. We also observed that the overestimation was higher at the early stage of crop growth when compared to the more advanced stages. Since the volume powers were computed with a similar strategy as proposed in [35], the volume components were equal for both decomposition approaches.

To understand the growing vegetation scenario, we looked at the CP data-derived CpRVI and other distance based measures during the crop growth cycle ($D1$, $D2$, and $D3$), as shown in Fig. 4 for a soya field. We utilized the Kennaugh matrix of an ID, a realization of vegetation canopy, as a volume model to determine the proximity of an observed target Stokes vector to a randomly polarized wave. In this regard, we looked at the temporal change in the GD and similarity measure with respect to ID [38]. The decreasing distance from the ID (and consequently increasing similarity measure) indicated the growing depolarizing tendency over the agricultural fields as a result of the crop growth. At an early stage of crop growth, when the lower range of CpRVI prevails (nearly bare field conditions), the polarized surface power component is expected to predominate. However, under practical field scenarios, the polarized component of the scattered power from bare agricultural fields may not originate from a pure surface (or odd bounce) scattering. An even or odd bounce scattering is determined by the electromagnetic interaction of the incoming radar signal with the target characteristics matching the order of the incident wavelength.

The compensated powers are presented in Figs. 6 and 8 for both real and simulated hybrid CP data, respectively. Comparison of pre- and postcompensated powers, as can be observed in Figs. 3 and 6(a), indicates a significant reduction in the overestimated double bounce component. In both cases (real and simulated hybrid CPs) presented in Figs. 6 and 8, the proposed decomposition closely followed the decomposed powers obtained from [35]. Under bare field condition ($D1$ in Fig. 8), the double bounce power in the proposed decomposition is slightly higher than [35] for both soya and corn fields. Samples originating from a single bounce scattering (bare soil vegetation-free condition) are expected to be concentrated on the south pole of the Poincaré sphere. On the contrary, some intrasample dispersion seems to be apparent between the samples originating from different portions of the bare soya field in Manitoba, Canada [Fig. 2(a)], which can be visually appreciated in Fig. 7(a) with the Poincaré sphere representation. The target irregularities from different sections of the field appear to be the factor contributing to the increase in the pseudo-double bounce power. Therefore, the distance based decomposition approach appears to be more sensitive to the sample dispersion when compared to the decomposition utilizing the roll-invariant scattering-type parameters [35]. This explains the necessity for the inclusion of a compensation factor in the proposed decomposition.

Investigations proposing/utilizing CP decomposition techniques have predominantly presented the averaged values of decomposition powers over a region of interest for highlighting the effectiveness of the decomposition in capturing the temporal change in the target scattering. However, such investigations have seldom reported any visual nuances between the real and simulated hybrid CP data. Therefore, we utilized the Poincaré sphere representation [50], [51] for observing the changes in the scattering scenarios occurring over the agricultural fields as a result of the temporal

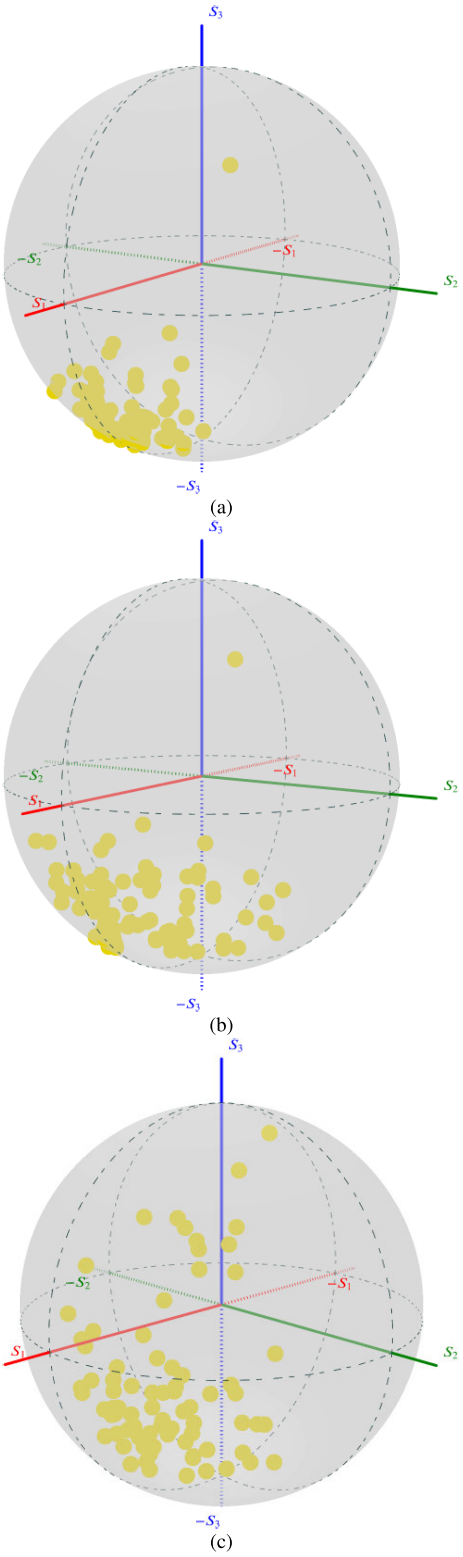

Fig. 5. Poincaré sphere representation of changing scattering scenario with the temporal progression of crop growth over a soya field in Sherbrooke, QC, Canada, 2022. (a) June ($D1$). (b) July ($D2$). (c) August ($D3$). The corresponding decomposition powers are shown in Fig. 6(a) and (b), respectively. Each point in the Poincaré sphere represents a field pixel. Observations for RCM real hybrid CP data.

progression of the crop growth. Moreover, the idea of GD aligns well with the spherical representation of the CP data. By virtue of this representation, we noticed unique visual nuances between real and simulated hybrid CP data in terms of the trend of temporal changes in the scattering behavior, as shown in Figs. 5 (with the corresponding decomposition in Fig. 6) and 7 (with the corresponding decomposition in Fig. 8). The sample dispersion is more evident over the Sherbrooke site (RCM) when compared to the Manitoba site (RS2). Differing ranges of incidence angles for RCM (ScanSAR: 17.03°–21.90°) and RS2 (FQ15W: 33.78°–36.37°) data can possibly influence this observation.

This representation effectively captures the overall scattering scenario over a region of interest since each sample point on the surface/within the Poincaré sphere essentially defines the state of polarization of a single pixel [52], [53].

With real compact data, the scattering mechanism evolves from nearly circularly polarized (where the samples are clustered at the south pole of the Poincaré sphere) to elliptically polarized waves that skim along the curvature of the sphere. During the very early stage of the growing season, while the leaf development and stem elongation are still in progress, a left-handed circular response (sample cloud is concentrated on the south pole) dominates. As the crop growth progresses, the dominant component of the surface scattering decreases [54]. The sample cluster traverses from the south pole toward the equator and eventually disperses within the Poincaré sphere, inducing a diverse range of ellipticities and DoPs. The sample cloud movement within the sphere illustrates the variation of ellipticity, orientation, and handedness of the backscattered wave as crops undergo changes in phenology. The presence of ellipticity in the backscattered wave indicates the occurrence of budding and flowering. When a certain orientation of polarization (H or V) is selectively attenuated, the backscattered wave develops linearity. The orientation of the elliptical or linear component depends on the arrangement and dimension of the canopy element. The growing vertical canopy orientation within the vegetation volume results in the increase in the double bounce scattering component [55]. In the advanced stage of crop growth, canopy element arrangement can be represented by the random distribution of dipole scatterers contributing to the volume scattering component [56]. The complex canopy arrangement is reflected by the randomness in the wave scattering parameters (like orientation). Due to the rising volume scattering contribution and limited penetration capability of the C-band, the signal contribution from the surface decreases [54], [57]. Upon crop harvest, the sample cloud is expected to return to the left-handed circular wave scattering. Such variations are sensitive both to the crop phenology (its stages of evolution) and crop type [58]. In the case of the simulated hybrid CP data, this trend of the cluster of points skimming along the curvature of the Poincaré sphere appears to be absent (Fig. 7). On the contrary, samples from the field at an early growth stage are located around the pole with some intrasample dispersion, similar to the real hybrid CP data, and as the crop growth progresses the cluster moves toward the equator in a vertical manner (rather than bending along the curvature of the sphere). This movement depicts the increasing level of randomness between the points in the sample cloud as the crop growth progresses. Therefore, as the vegetation grows, the cluster

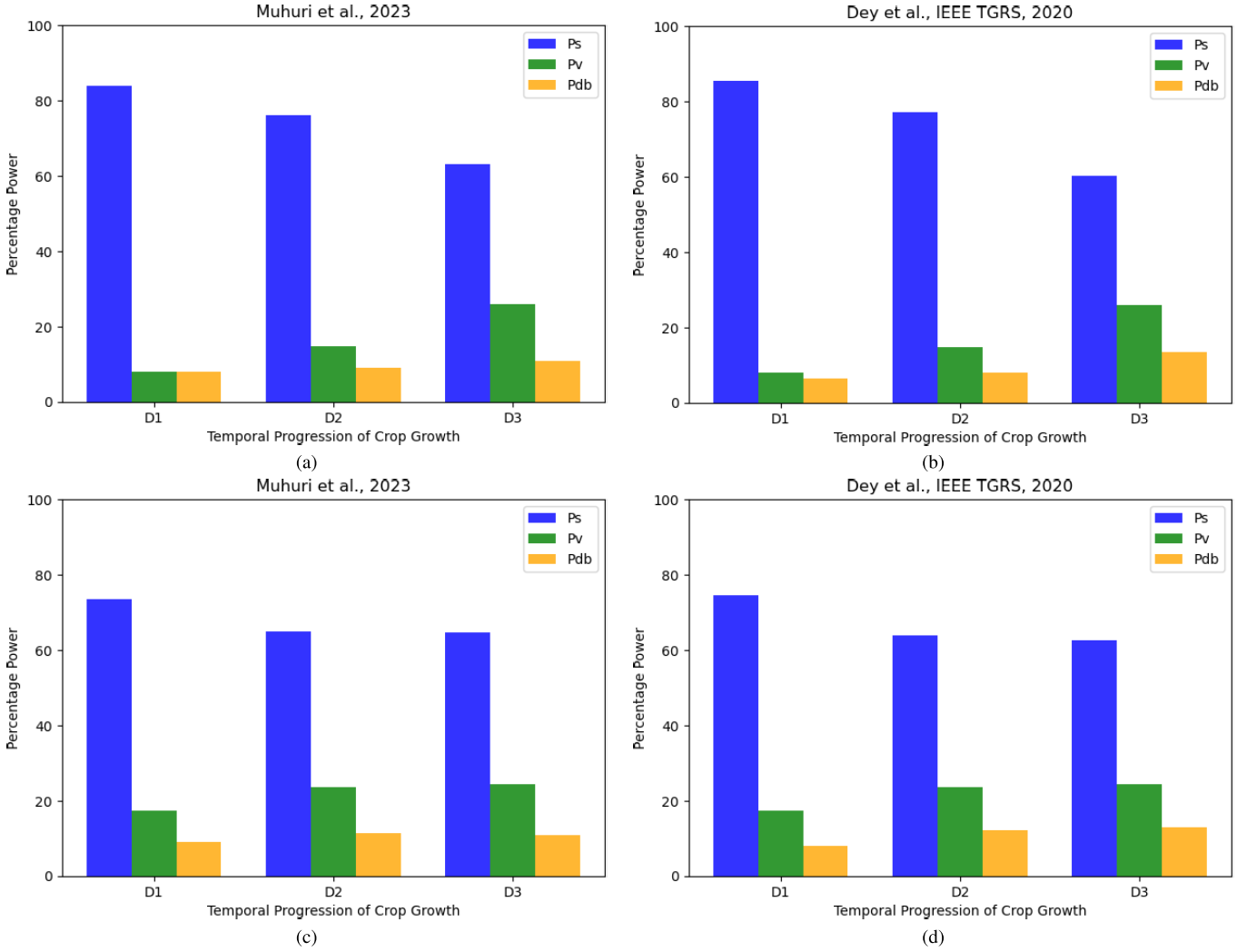

Fig. 6. Comparison of decomposition powers: proposed versus Dey et al. [35] IEEE TGRS, 2020. $D1$: June, $D2$: July, and $D3$: August indicate the temporal progression of crop growth over Sherbrooke, QC, Canada, 2022. (a) and (b) Soya. (c) and (d) Corn. The powers are averaged over an agricultural field. Observations for RCM real hybrid CP data.

appears more dispersed due to the differences in the vegetation characteristics at different sections of the agricultural field. Thus, the observed randomness within the Poincaré sphere is caused due to unique differences, introduced as a result of crop growth, in the scattering mechanisms within an agricultural field of the same crop type.

At an early stage ($D1$), the placement of the sample cluster within the sphere (near the poles with almost zeros ellipticity or between the poles and the equator with finite ellipticity) is sensitive to the state of the bare field (lightly vegetated), which can be appreciated by comparing Fig. 1 with Fig. 2 and Fig. 5 with Fig. 7. Furthermore, it is interesting to note that crop growth and movement of the sample cluster within the Poincaré sphere are strongly correlated until the fields attain a certain stage of crop biomass beyond which further transition of the sample appears to be relatively random. CP return from the bare fields is expected to be nearly circular with the sample cloud clustering around the south pole. As the vegetation develops, the transmitted polarimetric phase between the horizontal and vertical components is perturbed and the amplitude of each polarization channel is selectively attenuated as per the orientation and dielectric state of the scattering elements. An increase in the randomness/deviations in the ellipticities in the sample cloud contributed to an increase in the volume scattering power, which can be observed in the advanced stages ($D3$) of crop growth in Figs. 6 and 8. Thus, an increase in the volume power can be attributed to an enhanced level of randomness/dispersion of the samples within the Poincaré sphere. It is also interesting to observe that higher percentages of volume powers, as can be observed in Fig. 8 as compared to Fig. 6, corresponds to clustering of the sample cloud around the origin of the Poincaré sphere indicating the presence of strongly depolarizing targets, which is apparent in Fig. 7. In both cases (real and simulated hybrid CPs), despite the nuances in the scattering behavior, as observed in the Poincaré sphere representation, the decompositions (proposed and [35]) were able to reliably capture the progression of the crop growth through the scattering powers. These nuances can be attributed to the inherent differences in the imaging architectures followed by FP and hybrid CP systems with regard to transmit and receive polarization basis.

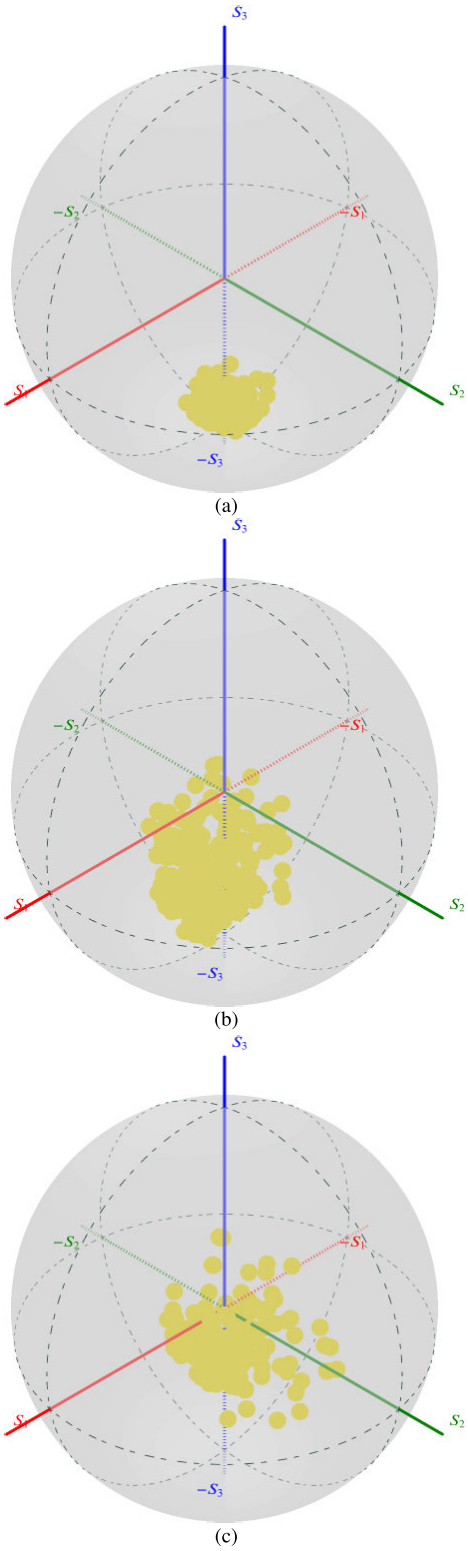

Fig. 7. Poincaré sphere representation of changing scattering scenario due to temporal progression of crop growth over a soya field in Carman, MB, Canada, 2016. (a) May ($D1$). (b) June ($D2$). (c) July ($D3$). The corresponding decomposition powers are shown in Fig. 8(a) and (b), respectively. Each point in the Poincaré sphere represents a field pixel. Observations for RS2 simulated hybrid CP data.

V. Discussion

In this investigation, we demonstrated the potential of GD (between the Kennaugh matrices of the observed and canonical targets) to decompose CP SAR data acquired over agricultural landscapes. The RCM CP radar architecture transmitted a right-circularly polarized SAR signal, so a bare surface or odd bounce scattered wave was returned in the opposite sense as a left-circular polarized wave. We decomposed the polarized portion of the total power in proportion to the similarity (or proximity) measure to the canonical targets (dihedral or trihedral). The technique was observed to be effective for monitoring the temporal changes in the scattering powers occurring as a result of progression in crop growth.

Since we proposed a GD-based CP decomposition in this investigation, it was necessary to obtain the CP form of the target Kennaugh matrix to be able to characterize the polarimetric scattering information (via geodesic proximity to the canonical scatterers). It is possible that a Kennaugh matrix constructed with a limited number of elements may not be the ideal way to fully characterize a target scattering scenario. However, it is important to note that the Kennaugh matrix representation in terms of the elements of the Stokes vector utilized the complete information present in the Stokes vector. Although the target characterization abilities of CP data is a matter of constant debate in the Earth observation community, the CP system enables enhanced swath observations (better spatial and temporal coverages) when compared to FP SAR sensors.

With a preliminary distance based decomposition, we observed an overestimation of the double bounce powers and an underestimation of the surface powers. Therefore, we introduced the idea of a pseudo-power component arising from the interaction between the target irregularities and incident signal, prominently under bare field (lightly vegetated) conditions. Furthermore, we proposed a polarized power (surface and double bounce) compensation/readjustment factor to resolve this issue. The compensation factor was estimated by utilizing an exponentially decaying function of CpRVI to retrieve the pseudo-power component from the double bounce power. The CpRVI was utilized as an indicator of the prevailing vegetation condition over the agricultural fields and the degree of readjustment/compensation that was necessary. The effectiveness of the CpRVI in the compensation process demonstrated its potential to reliably capture the different phenological stages of crop growth. Moreover, we also tested the proposed technique by replacing the distance to the dihedral with the distance to the helix. However, this did not resolve the issue of pseudo-double bounce power. The proposed compensation factor based on the CpRVI was still necessary. In addition to the target irregularities, there may be several other factors (like an imbalance in the Stokes vector-derived Kennaugh matrix) contributing to the observed scattering bias.

It is important to reemphasize that the scattering bias (or pseudo-power) is not assumed to be arising from the vegetation but from the surface irregularities. The polarimetric vegetation indicator (CpRVI) was only utilized to quantify the progressively obscuring effect of the growing vegetation, which gradually concealed the surface irregularities from the imaging signal as the crop growth progressed. Therefore, we exponentially decreased the amount of compensation for the pseudo-power as a function of CpRVI since we associated

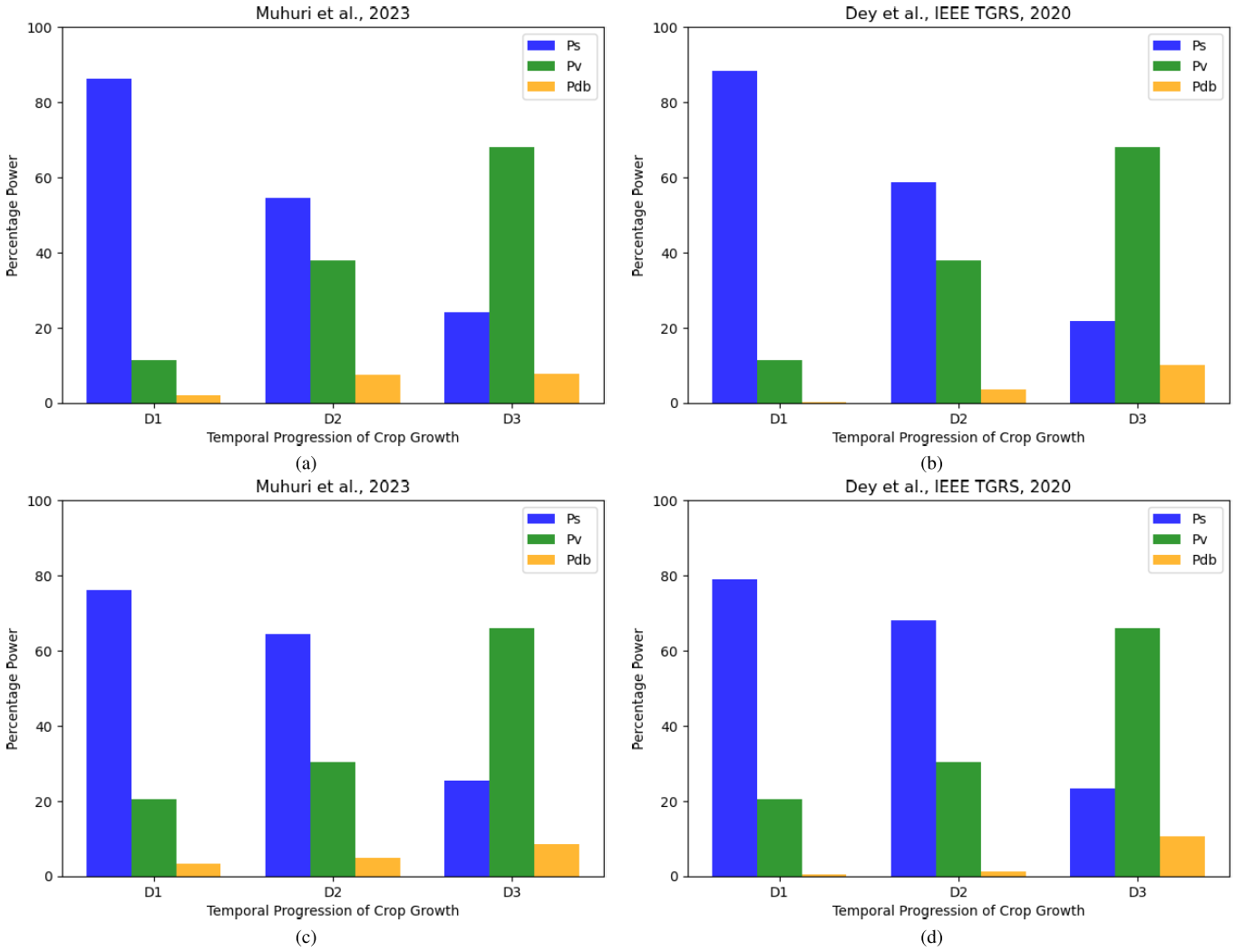

Fig. 8. Comparison of decomposition powers: proposed versus Dey et al. [35] IEEE TGRS, 2020. $D1$: May, $D2$: June, and $D3$: July indicate the temporal progression of crop growth over Carman, MB, Canada, 2016. (a) and (b) Soya. (c) and (d) Corn. The powers are averaged over an agricultural field. Observations for RS2 simulated hybrid CP data.

the extra power component with the surface irregularities and not with vegetation randomness. The important thing here was to adopt a decaying power function that attenuates the interaction between the target irregularities and the incident signal as a result of the temporal progression of vegetation growth. This occurs due to the progressively decreasing transmittivity of the incident signal through the fresh growing vegetation volume. Moreover, the rate of growth of vegetation is not linear over the cropping cycle. Therefore, we introduced an exponentially decreasing function to simulate the idea of decreasing signal–surface interaction. This is the physical justification that we would like to put forward for our assumption. Furthermore, in the advanced stages of crop growth, when the interaction between the target irregularities and the incident signal is limited, the CPRVI can be modulated by a constant $(\exp(-A_{\text{Vegetation}} * \text{CpRVI}))$, which is sensitive to the vegetation characteristics and prevailing biomass. This will effectively reduce the pseudo-power extracted from P_{DB} (beyond the 36.78% limit) under dense vegetation condition when the volume scattering is directed toward the soil, reflected by the soil, interact with the vegetation, and is then attenuated by the vegetation layer before reaching the sensor.

For the first time, we presented the visual nuances between the real and simulated hybrid CP data in the Poincaré sphere representation. While the real CP sample cloud largely followed the curvature of the sphere (Fig. 5), the simulated cloud indicated a vertical movement (Fig. 7) with the samples concentrated around the $S3$-axis. The difference in the range of incidence angles for the two sensors (RS2 acquisitions were at higher incidence angles when compared to RCM) possibly influenced this observation. The use of Poincaré sphere to demonstrate such differences are limited in the PolSAR literature [50], [59]. We explained the relationship between the dynamics of the sample cloud within the sphere and the decomposition powers. Such visual representations are necessary for a comprehensive and intuitive understanding of the target scattering dynamics while decomposing the total backscattered power over a region of interest. The perspective is otherwise incomplete when only the averaged values of the decomposed powers are presented, as is often the case in the literature. We observed that despite the nuances in the scattering behavior, both the decomposition techniques (proposed and Dey et al. [35] IEEE TGRS, 2020) were reliably able to capture the progression of crop growth in terms of temporal

change in the scattering powers. We observed that the proposed GD-based decomposition approach indicated a higher sensitivity to the nuances in the scattering behavior when compared to the other decomposition technique (Dey et al. [35] IEEE TGRS, 2020) that utilized the roll-invariant scattering-type parameters. Overall, the decomposition results were comparable for both cases (real and simulated hybrid CPs) considered in this investigation. During the early stage of the crop growth cycle, we observed relatively higher percentages of surface power over the soya fields when compared to the corn fields for both cases. This can be prominently attributed to target irregularities and, to a lesser extent, to the obscuring effect of higher crop biomass (at advanced stages) and crop height (as can be observed in Fig. 1), which consequently limits radar signal penetration and surface interactions [44], [60], [61].

It is important to appreciate the close proximity of compensated decomposition powers (in Figs. 6 and 8) obtained using fundamentally different decomposition approaches, which supported our assumption and demonstrated the effectiveness of the compensation. Although the acquisition of surface irregularity information would have been useful, it is not only challenging due to the manual efforts involved, but also impractical for operational applications and infeasible to measure at advanced stages of crop growth without destructing the crops. Detailed analysis and synchronization between the field measurements and satellite acquisition are necessary to establish such complex relationships. The authors are investigating the impact of various field conditions over the observed polarimetric response through their ongoing field campaign over the agricultural test site in Sherbrooke, QC, Canada.

VI. Conclusion

The following key observations can be concluded from this investigation.

1) We proposed a GD-based scattering power decomposition technique for CP SAR data acquired over agricultural landscapes. The technique incorporated a compensation factor that utilized the CpRVI to compensate for the pseudo-power (attributed to be arising from the target irregularities) observed in the double bounce component.
2) We presented the unique visual nuances between the real and simulated hybrid CP data in terms of temporal changes in radar scattering occurring as a result of crop growth. The Poincaré sphere representation was introduced as the quintessential visualization tool for providing a comprehensive overview of the nuances between the CP cases considered in this investigation.
3) Our proposed decomposition powers closely followed the recently proposed nonmodel-based three-component scattering power CP decomposition, which utilizes novel roll-invariant scattering-type parameters [35]. It is noteworthy that even though the two decomposition techniques followed different mathematical approaches to decompose the scattering powers, they indicated strong resemblance both in terms of the temporal trend (increasing or decreasing powers) and the proportion of distribution of the scattering powers between the decomposed components. Furthermore, the effectiveness of both decomposition techniques in capturing the progression of crop growth was not impacted by the nuances observed in the Poincaré sphere representation between the real and simulated hybrid CP data.

Acknowledgment

The authors would like to thank the Canadian Space Agency/Agence Spatiale Canadienne (CSA/ASC) for the satellite SAR time-series. We acknowledge the cooperation of Sherbrooke Research and Development Centre, AAFC for sharing their experimental facilities and agricultural sites. This research was financially supported by the Natural Science and Engineering Research Council of Canada (NSERC) Discovery grants (RGPIN-2017-05533 and RGPIN-2018-06101), Collaborative Research and Training Experience (CREATE) grant (543360-2020), and the Canadian Space Agency Class Grant and Contribution Program (21SUESAMMI) as part of the Canadian plan to spatial missions of soil moisture. We are grateful to Bhanu Prakash Mookkuthala Erkaramana (CARTEL, Département de Géomatique Appliquée, Université de Sherbrooke, Québec, Canada), Kurt Gottfried (Agriculture and Agri-Food Canada), Ridha Touzi (Canada Centre for Remote Sensing), Daniel De Lisle (CSA/ASC), Avik Bhattacharya (MRSL, IIT Bombay, India), Natascha Oppelt (EOM, CAU Kiel, Germany), and Kiel Marine Science (KMS) for their kind support. We thank the anonymous reviewers for their critical and constructive comments.

References

[1] S. R. Cloude and E. Pottier, "A review of target decomposition theorems in radar polarimetry," *IEEE Trans. Geosci. Remote Sens.*, vol. 34, no. 2, pp. 498–518, Mar. 1996.
[2] A. Freeman and S. L. Durden, "A three-component scattering model for polarimetric SAR data," *IEEE Trans. Geosci. Remote Sens.*, vol. 36, no. 3, pp. 963–973, May 1998.
[3] Y. Yamaguchi, T. Moriyama, M. Ishido, and H. Yamada, "Four-component scattering model for polarimetric SAR image decomposition," *IEEE Trans. Geosci. Remote Sens.*, vol. 43, no. 8, pp. 1699–1706, Aug. 2005.
[4] R. Touzi, "Target scattering decomposition in terms of roll-invariant target parameters," *IEEE Trans. Geosci. Remote Sens.*, vol. 45, no. 1, pp. 73–84, Jan. 2007.
[5] W. An, Y. Cui, and J. Yang, "Three-component model-based decomposition for polarimetric SAR data," *IEEE Trans. Geosci. Remote Sens.*, vol. 48, no. 6, pp. 2732–2739, Jun. 2010.
[6] J. J. van Zyl, M. Arii, and Y. Kim, "Model-based decomposition of polarimetric SAR covariance matrices constrained for nonnegative eigenvalues," *IEEE Trans. Geosci. Remote Sens.*, vol. 49, no. 9, pp. 3452–3459, Sep. 2011.
[7] Y. Cui, Y. Yamaguchi, J. Yang, H. Kobayashi, S.-E. Park, and G. Singh, "On complete model-based decomposition of polarimetric SAR coherency matrix data," *IEEE Trans. Geosci. Remote Sens.*, vol. 52, no. 4, pp. 1991–2001, Apr. 2014.
[8] R. Touzi, "Polarimetric target scattering decomposition: A review," in *Proc. IEEE Int. Geosci. Remote Sens. Symp. (IGARSS)*, Jul. 2016, pp. 5658–5661.
[9] T. Jagdhuber, I. Hajnsek, and K. P. Papathanassiou, "An iterative generalized hybrid decomposition for soil moisture retrieval under vegetation cover using fully polarimetric SAR," *IEEE J. Sel. Topics Appl. Earth Observ. Remote Sens.*, vol. 8, no. 8, pp. 3911–3922, Aug. 2015.
[10] S. Dey, A. Bhattacharya, A. C. Frery, C. López-Martínez, and Y. S. Rao, "A model-free four component scattering power decomposition for polarimetric SAR data," *IEEE J. Sel. Topics Appl. Earth Observ. Remote Sens.*, vol. 14, pp. 3887–3902, 2021.

[11] T. Kailath, "The divergence and Bhattacharyya distance measures in signal selection," *IEEE Trans. Commun.*, vol. COM-15, no. 1, pp. 52–60, Feb. 1967.

[12] P.-E. Danielsson, "Euclidean distance mapping," *Comput. Graph. Image Process.*, vol. 14, no. 3, pp. 227–248, Nov. 1980.

[13] W. L. Cameron and H. Rais, "Conservative polarimetric scatterers and their role in incorrect extensions of the Cameron decomposition," *IEEE Trans. Geosci. Remote Sens.*, vol. 44, no. 12, pp. 3506–3516, Dec. 2006.

[14] W. L. Cameron and H. Rais, "Polarization symmetric scatterer metric space," *IEEE Trans. Geosci. Remote Sens.*, vol. 47, no. 4, pp. 1097–1107, Apr. 2009.

[15] A. D. C. Nascimento, M. M. Horta, A. C. Frery, and R. J. Cintra, "Comparing edge detection methods based on stochastic entropies and distances for PolSAR imagery," *IEEE J. Sel. Topics Appl. Earth Observ. Remote Sens.*, vol. 7, no. 2, pp. 648–663, Feb. 2014.

[16] L. Torres, S. J. S. Sant'Anna, C. da Costa Freitas, and A. C. Frery, "Speckle reduction in polarimetric SAR imagery with stochastic distances and nonlocal means," *Pattern Recognit.*, vol. 47, no. 1, pp. 141–157, Jan. 2014.

[17] A. Bhattacharya, A. Muhuri, S. De, S. Manickam, and A. C. Frery, "Modifying the Yamaguchi four-component decomposition scattering powers using a stochastic distance," *IEEE J. Sel. Topics Appl. Earth Observ. Remote Sens.*, vol. 8, no. 7, pp. 3497–3506, Jul. 2015.

[18] C. R. Rao, "Information and the accuracy attainable in the estimation of statistical parameters," in *Breakthroughs in Statistics: Foundations and Basic Theory*. Springer, 1992, pp. 235–247. [Online]. Available: https://link.springer.com/chapter/10.1007/978-1-4612-0919-5_16

[19] L. Bombrun, N.-E. Lasmar, Y. Berthoumieu, and G. Verdoolaege, "Multivariate texture retrieval using the SIRV representation and the geodesic distance," in *Proc. IEEE Int. Conf. Acoust., Speech Signal Process. (ICASSP)*, May 2011, pp. 865–868.

[20] J. Naranjo-Torres, J. Gambini, and A. C. Frery, "The geodesic distance between G_I^0 models and its application to region discrimination," *IEEE J. Sel. Topics Appl. Earth Observ. Remote Sens.*, vol. 10, no. 3, pp. 987–997, Mar. 2017.

[21] A. Muhuri, S. Manickam, and A. Bhattacharya, "Scattering mechanism based snow cover mapping using RADARSAT-2 C-band polarimetric SAR data," *IEEE J. Sel. Topics Appl. Earth Observ. Remote Sens.*, vol. 10, no. 7, pp. 3213–3224, Jul. 2017.

[22] A. Muhuri, D. Ratha, and A. Bhattacharya, "Seasonal snow cover change detection over the Indian Himalayas using polarimetric SAR images," *IEEE Geosci. Remote Sens. Lett.*, vol. 14, no. 12, pp. 2340–2344, Dec. 2017.

[23] A. Muhuri, S. Manickam, A. Bhattacharya, and Snehmani, "Snow cover mapping using polarization fraction variation with temporal RADARSAT-2 C-band full-polarimetric SAR data over the Indian Himalayas," *IEEE J. Sel. Topics Appl. Earth Observ. Remote Sens.*, vol. 11, no. 7, pp. 2192–2209, Jul. 2018. [Online]. Available: https://scholar.google.com/scholar?hl=en&as_sdt=0%2C5&q=snehmani+sase&btnG=

[24] D. Ratha, S. De, T. Celik, and A. Bhattacharya, "Change detection in polarimetric SAR images using a geodesic distance between scattering mechanisms," *IEEE Geosci. Remote Sens. Lett.*, vol. 14, no. 7, pp. 1066–1070, Jul. 2017.

[25] O. Antropov, Y. Rauste, and T. Hame, "Volume scattering modeling in PolSAR decompositions: Study of ALOS PALSAR data over boreal forest," *IEEE Trans. Geosci. Remote Sens.*, vol. 49, no. 10, pp. 3838–3848, Oct. 2011.

[26] D. Ratha, D. Mandal, V. Kumar, H. Mcnairn, A. Bhattacharya, and A. C. Frery, "A generalized volume scattering model-based vegetation index from polarimetric SAR data," *IEEE Geosci. Remote Sens. Lett.*, vol. 16, no. 11, pp. 1791–1795, Nov. 2019.

[27] D. Mandal et al., "Assessment of rice growth conditions in a semi-arid region of India using the generalized radar vegetation index derived from RADARSAT-2 polarimetric SAR data," *Remote Sens. Environ.*, vol. 237, Feb. 2020, Art. no. 111561.

[28] G. E. Atteia and M. J. Collins, "On the use of compact polarimetry SAR for ship detection," *ISPRS J. Photogramm. Remote Sens.*, vol. 80, pp. 1–9, Jun. 2013.

[29] R. K. Raney, "Hybrid-polarity SAR architecture," *IEEE Trans. Geosci. Remote Sens.*, vol. 45, no. 11, pp. 3397–3404, Nov. 2007.

[30] J.-C. Souyris, P. Imbo, R. Fjortoft, S. Mingot, and J.-S. Lee, "Compact polarimetry based on symmetry properties of geophysical media: The $\pi/4$ mode," *IEEE Trans. Geosci. Remote Sens.*, vol. 43, no. 3, pp. 634–646, Mar. 2005.

[31] N. Stacy and M. Preiss, "Compact polarimetric analysis of X-band SAR data," in *Proc. EUSAR*, vol. 6, 2006, p. 4. [Online]. Available: https://www.vde-verlag.de/proceedings-en/562960201.html

[32] S. R. Cloude, D. G. Goodenough, and H. Chen, "Compact decomposition theory," *IEEE Geosci. Remote Sens. Lett.*, vol. 9, no. 1, pp. 28–32, Jan. 2012.

[33] R. K. Raney, J. T. S. Cahill, G. W. Patterson, and D. B. J. Bussey, "The *m-chi* decomposition of hybrid dual-polarimetric radar data with application to lunar craters," *J. Geophys. Res., Planets*, vol. 117, no. E12, Dec. 2012, Art. no. E00H21.

[34] A. Bhattacharya, S. De, A. Muhuri, M. Surendar, G. Venkataraman, and A. K. Das, "A new compact polarimetric SAR decomposition technique," *Remote Sens. Lett.*, vol. 6, no. 12, pp. 914–923, Dec. 2015.

[35] S. Dey, A. Bhattacharya, D. Ratha, D. Mandal, and A. C. Frery, "Target characterization and scattering power decomposition for full and compact polarimetric SAR data," *IEEE Trans. Geosci. Remote Sens.*, vol. 59, no. 5, pp. 3981–3998, May 2021.

[36] V. Kumar, D. Mandal, A. Bhattacharya, and Y. S. Rao, "Crop characterization using an improved scattering power decomposition technique for compact polarimetric SAR data," *Int. J. Appl. Earth Observ. Geoinf.*, vol. 88, Jun. 2020, Art. no. 102052.

[37] Q. Yin, J. Xu, D. Xiang, Y. Zhou, and F. Zhang, "Polarimetric decomposition with an urban area descriptor for compact polarimetric SAR data," *IEEE J. Sel. Topics Appl. Earth Observ. Remote Sens.*, vol. 14, pp. 10033–10044, 2021.

[38] D. Mandal et al., "A radar vegetation index for crop monitoring using compact polarimetric SAR data," *IEEE Trans. Geosci. Remote Sens.*, vol. 58, no. 9, pp. 6321–6335, Sep. 2020.

[39] S. N. Anfinsen, A. P. Doulgeris, and T. Eltoft, "Estimation of the equivalent number of looks in polarimetric synthetic aperture radar imagery," *IEEE Trans. Geosci. Remote Sens.*, vol. 47, no. 11, pp. 3795–3809, Nov. 2009.

[40] F. Nunziata, A. Gambardella, and M. Migliaccio, "On the Mueller scattering matrix for SAR sea oil slick observation," *IEEE Geosci. Remote Sens. Lett.*, vol. 5, no. 4, pp. 691–695, Oct. 2008.

[41] W. Fehr and C. Caviness, "Stages of soybean development," Cooperat. Extension Service, Agricult. and Home Econ. Exp. Station, Iowa State Univ. Sci. Technology, Ames, IA, USA, 1977. [Online]. Available: https://dr.lib.iastate.edu/entities/publication/58c89bfe-844d-42b6-8b6c-2c6082595ba3 and https://dr.lib.iastate.edu/server/api/core/bitstreams/13bd0d8f-66ff-4d0e-a0e3-a70c2c47f6f3/content

[42] L. J. Abendroth et al., "Corn growth and development," Iowa State Univ. Extension, Ames, IA, USA, Tech. Rep. PMR 10092011, 2011. [Online]. Available: https://www.researchgate.net/publication/280092215_In_Corn_Growth_and_Development

[43] E. M. Kennaugh, "Effects of the type of polarization on echo characteristics," Antenna Lab, Ohio State Univ., Columbus, OH, USA, Tech. Rep. 389-9, 1951.

[44] B. A. Campbell, "High circular polarization ratios in radar scattering from geologic targets," *J. Geophys. Res., Planets*, vol. 117, no. E6, Jun. 2012, Art. no. E06008.

[45] T. J. Jackson, K. G. Kostov, and S. S. Saatchi, "Rock fraction effects on the interpretation of microwave emission from soils," *IEEE Trans. Geosci. Remote Sens.*, vol. 30, no. 3, pp. 610–616, May 1992.

[46] M. M. Rahman et al., "Mapping surface roughness and soil moisture using multi-angle radar imagery without ancillary data," *Remote Sens. Environ.*, vol. 112, no. 2, pp. 391–402, Feb. 2008.

[47] D. Brunner, G. Lemoine, H. Greidanus, and L. Bruzzone, "Radar imaging simulation for urban structures," *IEEE Geosci. Remote Sens. Lett.*, vol. 8, no. 1, pp. 68–72, Jan. 2011.

[48] E. R. Jawin et al., "The relationship between radar scattering and surface roughness of lunar volcanic features," *J. Geophys. Res., Planets*, vol. 119, no. 11, pp. 2331–2348, Nov. 2014.

[49] S. Cloude, *Polarisation: Applications in Remote Sensing*. Oxford, U.K.: OUP, 2009.

[50] F. Shang and A. Hirose, "Quaternion neural-network-based PolSAR land classification in Poincaré-sphere-parameter space," *IEEE Trans. Geosci. Remote Sens.*, vol. 52, no. 9, pp. 5693–5703, Sep. 2014.

[51] N. Usami, A. Muhuri, A. Bhattacharya, and A. Hirose, "Proposal of wet snowmapping with focus on incident angle influential to depolarization of surface scattering," in *Proc. IEEE Int. Geosci. Remote Sens. Symp. (IGARSS)*, Jul. 2016, pp. 1544–1547.

[52] H. Poincare, *Theorie Mathematique de la Lumiere*, vol. 2. Paris, France: Gauthier-Villars, 1892.

[53] G. Milione, H. Sztul, D. Nolan, and R. Alfano, "Higher-order Poincaré sphere, Stokes parameters, and the angular momentum of light," *Phys. Rev. Lett.*, vol. 107, no. 5, 2011, Art. no. 053601.

[54] G. G. Ponnurangam and Y. S. Rao, "The application of compact polarimetric decomposition algorithms to L-band PolSAR data in agricultural areas," *Int. J. Remote Sens.*, vol. 39, no. 22, pp. 8337–8360, Nov. 2018.

[55] Z. Yang, K. Li, L. Liu, Y. Shao, B. Brisco, and W. Li, "Rice growth monitoring using simulated compact polarimetric C band SAR," *Radio Sci.*, vol. 49, no. 12, pp. 1300–1315, Dec. 2014.
[56] T. L. Ainsworth, J. P. Kelly, and J.-S. Lee, "Classification comparisons between dual-pol, compact polarimetric and quad-pol SAR imagery," *ISPRS J. Photogramm. Remote Sens.*, vol. 64, no. 5, pp. 464–471, Sep. 2009.
[57] G. G. Ponnurangam, T. Jagdhuber, I. Hajnsek, and Y. S. Rao, "Soil moisture estimation using hybrid polarimetric SAR data of RISAT-1," *IEEE Trans. Geosci. Remote Sens.*, vol. 54, no. 4, pp. 2033–2049, Apr. 2016.
[58] L. D. Robertson, H. McNairn, C. McNairn, S. Ihuoma, and X. Jiao, "Compact polarimetry for operational crop inventory," in *Proc. IEEE Int. Geosci. Remote Sens. Symp. (IGARSS)*, Jul. 2022, pp. 4423–4426.
[59] L. D. Robertson, H. McNairn, X. Jiao, C. McNairn, and S. O. Ihuoma, "Monitoring crops using compact polarimetry and the RADARSAT constellation mission," *Can. J. Remote Sens.*, vol. 48, no. 6, pp. 793–813, Nov. 2022.
[60] D. L. Evans, T. G. Farr, J. J. van Zyl, and H. A. Zebker, "Radar polarimetry: Analysis tools and applications," *IEEE Trans. Geosci. Remote Sens.*, vol. 26, no. 6, pp. 774–789, Nov. 1988.
[61] A. Muhuri, K. Goïta, R. Magagi, and H. Wang, "Soil moisture retrieval during crop growth cycle using satellite SAR time-series," *IEEE J. Sel. Topics Appl. Earth Observ. Remote Sens.*, early access, May 26, 2023, doi: 10.1109/JSTARS.2023.3280181.

Arnab Muhuri holds a Bachelors in Electrical Engineering (2009) and later obtained his Master of Technology (2012) & Ph.D. (2018) in Satellite Earth Observation from the Indian Institute of Technology (IIT) Bombay, India. In 2018, for his research contributions, he was conferred upon the Excellence in Ph.D. Research Award by the Honorable Prime Minister of India, Shri. Narendra Modi, at the 56th Institute Convocation of IIT Bombay, India.

In 2019, he was awarded the Alexander von Humboldt (AvH) Fellowship by the AvH Foundation, Government of the Federal Republic of Germany, to continue his research at the Professur für Hydrogeographie und Klimatologie, Geographisches Institut, Universität Heidelberg. In 2020, he was awarded the European Research Stay Grant by the AvH Foundation for working as a Visiting Scientist at the Centre d'Etudes Spatiales de la Biosphére (CESBIO)-Centre National d'Etudes Spatiales (CNES), Toulouse, France. In 2021, he joined the Centre d'Applications et de Recherches en Télédétection (CARTEL) at L'Université de Sherbrooke, Québec, Canada where his research was funded by the Discovery grant and CREATE program of the Natural Sciences and Engineering Research Council of Canada (NSERC). In 2022, he joined the Earth Observation and Modelling (EOM), Geographisches Institut, Christian-Albrechts-Universität zu Kiel, Germany, where he is working towards his Habilitation and teaches courses on satellite Earth observation. His present research interests lies in the development of Earth observation algorithms integrating fundamentals of imaging physics with information retrieval techniques like machine learning for applications like grassland and coastal monitoring with SAR, LiDAR, and optical sensors.

Dr. Muhuri has collaboratively worked with the Space Application Center (SAC), Indian Space Research Organisation (ISRO), and Defence Research & Development Organisation (DRDO), Ministry of Defence, Government of India. He was a Visiting Fellow at the University of Tokyo, Japan under the DST-JSPS grant. Dr. Muhuri has worked with Earth observation (RADARSAT-2 and RADARSAT Constellation Mission (RCM)) and extra-terrestrial (Chandrayaan-1 Mini-SAR) satellite missions for interdisciplinary applications like exploration of the Lunar polar regions, high-mountain cryosphere monitoring, natural disaster impact assessment, agricultural parameter retrieval, and development of polarimetric SAR decomposition techniques. He is on the review board of IEEE TGRS & JSTARS, International Journal of Climatology, Remote Sensing of Environment etc. and serves as a Research Ambassador for Heidelberg Alumni International, Universität Heidelberg.

Kalifa Goïta received the Engineering degree in surveying engineering from the École Nationale d'Ingénieurs, Bamako, Mali, in 1987, and the M.Sc. and Ph.D. degrees in remote sensing from the Université de Sherbrooke, Sherbrooke, QC, Canada, in 1991 and 1995, respectively.

He worked as a Post-Doctoral Fellow with the Climate Research Branch of Environment Canada, Toronto, ON, Canada, from 1995 to 1997. From 1997 to 2002, he was with the Faculty of Forestry, Université de Moncton, Moncton, NB, Canada, as a Professor of remote sensing and Geographic Information System (GIS). Since June 2002, he has been a Professor of geomatics with the Université de Sherbrooke, where he was the Head of the Department of Applied Geomatics from 2009 to 2014, and has been the Director of the Remote Sensing Research Centre (Centre d'Applications et de Recherches en Télédétection, CARTEL) since 2015. He has supervised/co-supervised numerous master's, Ph.D. students, and post-doctoral researchers, and is the author/coauthor of several research articles in the broad field of environmental remote sensing and water resources. His research interests include environmental geomatics, microwave remote sensing of soil moisture and snow, as well as satellite gravimetry and altimetry applied to water resources.

Ramata Magagi received the B.Sc. degree in physics from the Université de Niamey, Niamey, Niger, in 1989, and the M.Sc. and Ph.D. degrees in physics and chemistry of environment from the Institut National Polytechnique de Toulouse, Toulouse, France, in 1992 and 1995, respectively.

She is currently a Professor with the Department of Applied Geomatics, Université de Sherbrooke, Sherbrooke, QC, Canada. She led the Canadian Experiment for Soil Moisture in 2010 (CanEx-SM10). Her research activities include active and passive microwave remote sensing of soil, snow, vegetation, and precipitation.

Hongquan Wang received the B.Sc. degree in geographic information systems from the Northeast Forestry University, Harbin, China, in 2007, the M.Sc. degree in silviculture (forest remote sensing) from the Chinese Academy of Forestry, Beijing, China, in 2010, and the Ph.D. degree in synthetic aperture radar (SAR) remote sensing from the National Institute of Applied Sciences, IETR CNRS-6164, Rennes, France, in 2014.

He was involved in several scientific projects in the framework of CNRS Zone Atelier Armorique in France. From 2014 to 2018, he worked as a Post-Doctoral Fellow with the Center for Research and Application of Remote Sensing (CARTEL), University of Sherbrooke, Sherbrooke, QC, Canada, where he participated in the Soil Moisture Active Passive Validation Experiments in 2012 and 2016. From 2018 to 2021, he worked as an Assistant Professor with the Department of Environment and Resource Science, Zhejiang University, Hangzhou, China. As a Principal Investigator, he led several research programs to develop remote-sensing models, algorithms, and applications to characterize hydrosphere, cryosphere, biosphere, ecosystem, and climate changes. Since 2021, he has been working as a Researcher at the University of Sherbrooke and then at Agriculture and Agri-Food Canada (AAFC). His research interests include the development of multisource remote sensing (radar, radiometer, multispectral, hyperspectral, and LiDAR) methodologies (e.g., polarimetric decompositions and radiative transfer models) and applications to characterize the dynamics of the Earth systems.